

**Neutron pick-up pion transfer reactions
for
the formation of deeply bound pionic atoms in ^{208}Pb**

S. Hirenzaki^{a)} and H. Toki^{b)}

a) Department of Physics, Nara Women's Univ., Nara 630, Japan

b) Research Center for Nuclear Physics, Osaka Univ., Ibaraki, Osaka 567, Japan

ABSTRACT

We study (n, d) and $(d, ^3\text{He})$ reactions on ^{208}Pb leading to deeply bound pionic atoms with one neutron hole being left. We develop a theoretical model to calculate cross sections of deeply bound pionic atoms and quasi-elastic pion production. The results are compared with data which have been obtained so far. We show that the theoretical model describes the data of both reactions well.

1. Introduction

Since the suggestion of Toki and Yamazaki for the formation of deeply bound pionic atoms such as $1s$ and $2p$ states in heavy nuclei using direct reactions,^{1,2} there have been a number of experimental attempts to find these states. These states have a pionic halo structure due to a strong repulsive pion-nucleus interaction, which saves a pion from being absorbed by the nucleus.^{1,2} The (n, p) pion transfer reactions on ^{208}Pb at $T_n = 420\text{MeV}$ were measured by Iwasaki *et al.* using the Charge Exchange facility at TRIUMF.³ No evidence for pionic atoms was found, the reason for which was interpreted as due to large momentum mismatch at the nuclear surface where the pion transfer reaction takes place. A similar conclusion was made for $(d, ^2\text{He})$ reactions performed at SATURNE.⁴ It was then concluded that the pion transfer reactions of this type were not suited for the formation of deeply bound pionic atoms.³ The same conclusion was obtained also by Nieves and Oset.⁵

Different reactions were studied theoretically by other authors. Nieves and Oset

studied the reactions induced by leptons such as (γ, π^+) ⁶ and (e, e') .⁷ They studied also (Σ, Λ) reactions in order to reduce the momentum mismatch occurring in (n, p) reactions by reducing the Q-value due to the $\Sigma - \Lambda$ mass difference.⁸ Their latest suggestion on the use of low energy in-flight pion is also worth-mentioning, in which a photon after the direct capture of the in-flight π^- in deeply bound pionic states can be observed.⁹

Toki *et al.*, on the other hand, pushed further the use of the neutron and deuteron beams, but added another nucleon to participate in the pion transfer process; pion transfer followed by one nucleon pick up reactions such as (n, d) and $(d, {}^3\text{He})$.^{10,11} We show the schematic diagram for $(d, {}^3\text{He})$ reaction leading to pionic bound states in Fig. 1. These processes have an advantage to be able to choose the incident energy so as to make the reaction recoilless. In this kinematics, the pion carries a small momentum into the target nuclear system. Although the (n, d) and $(d, {}^3\text{He})$ reactions lead to complicated nuclear configurations together with the formation of pionic atoms, the recoilless condition may make the process experimentally feasible. In fact, the cross sections leading to pionic states (n, l) together with a neutron hole states of the same orbital angular momentum ('quasi' substitutional configurations, $\Delta l = 0$) were shown to be enhanced.^{10,11}.

The first attempt with the use of (n, d) reactions was performed by Trudel *et al.* with the Chargex facility at TRIUMF.¹² The zero degree experimental data was reported by Yamazaki at the International Nuclear Physics Conference (INPC).¹³ The forward double differential cross section for the ${}^{208}\text{Pb}(n, d)$ reaction at $T_n = 400\text{MeV}$ was measured with the experimental energy resolution of about 1MeV . In this experiment we observe that the cross section begins to increase gradually from flat background at the excitation energy corresponding to about 10MeV below the pion production threshold, not at the pion production threshold. This strength below the pion production threshold was expected to come from the deeply bound pionic atom formation. Matsuoka *et al.* measured cross sections of (p, pp) reactions to observe the deeply bound pionic atoms and obtained the similar spectrum to that of the (n, d) reactions.¹⁴ Thus, following the theoretical predictions,¹¹ the experimental search for deeply bound pionic atoms by $(d, {}^3\text{He})$ reactions was performed in order to improve

the data quality using the excellent deuteron beam. Yamazaki *et al.* performed an experiment very recently at GSI and reported that they found a clear peak structure due to deeply bound pionic atom formation.¹⁵ The agreement between the data and the theoretical prediction was found very good and this fact demonstrated that the theoretical model describes the reaction very well.

In this paper we study the one nucleon pick-up reaction leading to deeply bound pionic atoms theoretically. The calculated results are compared with data obtained recently. In section 2, we describe the formalism of calculating the (n, d) and $(d, {}^3\text{He})$ cross sections leading to pionic atoms and the pionic continuum states within the effective number approach. In section 3, we show general features of the one nucleon pick-up pion transfer reactions by considering (n, d) reactions. We present the calculated results of (n, d) reactions and compare them with the data. The $(d, {}^3\text{He})$ reaction is studied in section 4. Section 5 is devoted for summary and discussions.

2. Theoretical Model

In this section, we describe our theoretical model which was developed to calculate the (n, d) and $(d, {}^3\text{He})$ reactions leading to deeply bound pionic atoms. Since we are interested in the energy spectra only around the pion production threshold, we postulate that the spectrum depends on the energy only through three pionic processes; (1) bound π^- production, (2) quasi-elastic π^- production, and (3) quasi-elastic π^0 production. There is a neutron hole for π^- production processes and a proton hole for a π^0 production process in the final state. Other processes are assumed to be independent of the energy in this narrow region. In the previous publications, we have developed the effective number approach to calculate the bound π^- production process.^{10,11} In this section we describe our model including quasi-elastic processes.

The (n, d) cross sections for the nuclear target are written in the effective number approach as

$$\left(\frac{d^2\sigma}{d\Omega dE} \right)_{nA \rightarrow d(A-1)\pi} = \left(\frac{d\sigma}{d\Omega} \right)_{nn \rightarrow d\pi}^{lab} \sum_{l_\pi, j_n, J} \left(\frac{\Gamma}{2\pi} \frac{N_{eff}}{(\Delta E)^2 + \Gamma^2/4} + \frac{2}{\pi} E_\pi p_\pi N_{eff} \right) \quad (1)$$

with

$$N_{eff} = \frac{1}{2} \sum_{M,m_s} \left| \int \chi_f^*(\vec{r}) \xi_{\frac{1}{2},m_s}^*(\sigma) [\phi_{l_\pi}^*(\vec{r}) \otimes \psi_{j_n}(\vec{r}, \sigma)]_{JM} \chi_i(\vec{r}) d^3r d\sigma \right|^2 \quad (2)$$

The first term in Eq. (1) corresponds to the formation of pion bound states and the second one to unbound states. The ΔE in the first term is defined as $\Delta E = Q + m_\pi - B_\pi + S_n - 3.519 MeV$ for the (n, d) reactions with the pion binding energy (B_π), the neutron separation energy (S_n), and the reaction Q-value so as to make a peak structure at a resonance energy of each configuration of pion-particle neutron-hole state.¹⁰ For the $(d, {}^3\text{He})$ reactions we need to use $6.787 MeV$ instead of $3.519 MeV$ that appeared above.¹¹ The Γ denotes the width of the bound pionic state. The pion binding energies and widths are calculated using the realistic optical potential ². To calculate neutron separation energies for deep neutron states we use the potential parameters determined by Speth *et al.*¹⁶. We use experimental values for S_n when they are available. The E_π in the second term is the energy of unbound pions in the laboratory frame defined as $E_\pi = -Q - S_n + 3.519 MeV$ for π^- production in (n, d) reactions and p_π is the corresponding pion momentum. The factor $\frac{2}{\pi} E_\pi p_\pi$ is due to the phase volume of the unbound pion. The quasi elastic π^0 production is included in a similar way. The elementary cross section $(d\sigma/d\Omega)_{nn \rightarrow d\pi}$ is derived from the $pp \rightarrow d\pi^+$ cross sections by using the charge conjugation. In the $(d, {}^3\text{He})$ reactions, we need to use $(d\sigma/d\Omega)_{dp \rightarrow t\pi^+}$ as the elementary cross section. We show the elementary cross sections in Fig. 2.¹⁰

The ϕ_{l_π} and ψ_{j_n} in N_{eff} are the pion and the neutron hole wave functions with a resultant angular momentum J . The pion wave function is calculated by solving the Klein-Gordon equation with the realistic potential ². We use the harmonic oscillator wave function for the neutron wave function for simplicity. The spin wave function $\xi_{\frac{1}{2},m_s}$ with averaging over m_s is to take care of the possible spin directions of the neutrons in the target. The χ 's denote the initial and the final distorted waves of the projectile and the ejectile, which are treated in the eikonal approximation.¹⁰

The treatment of deeply bound pionic states is described in detail in previous publication.^{10,11} We describe here the quasi-elastic pion production part. The scattering pionic states are obtained by solving the Klein-Gordon equation with the finite Coulomb potential and the optical potential V_{opt} , which is written as

$$\begin{aligned}
2\bar{\omega}V_{opt} = & -4\pi[b(r) + B(r)] + 4\pi\vec{\nabla} \cdot \{L(r)[c(r) + C(r)]\}\vec{\nabla} \\
& - 4\pi\left\{\frac{p_1-1}{2}\nabla^2c(r) + \frac{p_2-1}{2}\nabla^2C(r)\right\}, \tag{3}
\end{aligned}$$

where

$$b(r) = p_1[\bar{b}_0\rho(r) - \varepsilon_\pi b_1(\rho_n(r) - \rho_p(r))], \tag{4}$$

$$\bar{b}_0 = b_0 - \frac{3k_F}{2\pi}(b_0^2 + 2b_1^2), \tag{5}$$

$$c(r) = p_1^{-1}[c_0\rho(r) - \varepsilon_\pi c_1(\rho_n(r) - \rho_p(r))], \tag{6}$$

$$B(r) = p_2 B_0 \rho^2(r), \tag{7}$$

$$C(r) = p_2^{-1} C_0 \rho^2(r), \tag{8}$$

$$L(r) = \left\{1 + \frac{4\pi}{3}\lambda[c(r) + C(r)]\right\}^{-1}. \tag{9}$$

The kinematical factors are defined as;

$$p_1 = 1 + \omega/M, \tag{10}$$

$$p_2 = 1 + \omega/2M, \tag{11}$$

and the reduced energy $\bar{\omega}$ is given by

$$\bar{\omega} = \omega/(1 + \omega/AM), \tag{12}$$

where ω is the pion total energy, ε_π is the pion charge, A is the nuclear mass number, and M is the nucleon mass. The potential is taken from Stricker *et al.*²², which has

been obtained by fitting to the pion nucleus elastic scattering cross sections. We show the potential parameters in Table 1. Needless to say, but the Coulomb potential is strongly attractive for the negative pions, while it is not present for the neutral pion. The Klein-Gordon equation is solved by multipole expansion for all the necessary partial waves and the relevant pion energies.

3. Numerical Results on (n, d) reactions

In this section we will show general features of the one nucleon pick-up pion transfer reactions by considering (n, d) cases. We would like to first study the threshold behavior of the (n, d) reactions leading to π^- and π^0 states. First of all, we show in Fig. 3 the pion wave functions for $l = 0$ at $T_\pi = 5\text{MeV}$ obtained by solving the Klein-Gordon equation with and without the optical potential as an example. It is important to note that the negative pion feels a strong Coulomb attraction, while the neutral pion does not. This difference makes a large difference in the behaviors of the pion wave functions in the nuclear region as depicted in Fig. 3. Without the optical potential, the neutral pion wave function is the spherical Bessel function (j_0). The negative pion wave function is pulled in to the small r region relative to the π^0 wave function as seen in Fig. 3 (a). By introduction of the optical potential, the central components of the wave functions are largely pushed outwards for both the negative and neutral pions as seen in Fig.3 (b). The large difference remains in the nuclear interior region. We comment here that these wave functions provide good elastic scattering cross sections.²²

These wave functions are then used in eq. (2) for N_{eff} at various pion energies. In order to calculate the energy spectra in the pion unbound region, we have to calculate cross sections for many final sates of the final nucleus ^{207}Pb . As a typical case, we show in Fig. 4 the quasi-elastic pion production cross sections for the cases of relatively large cross sections for π^- and π^0 starting from the pion threshold energy. Note that the hole states are neutrons for π^- and protons for π^0 . This figure clearly shows the large difference between the threshold behaviors of negative and neutral pion formation cross sections. The cross section for negative pion production at the threshold is finite, which smoothly connects to the finite cross sections in the bound

pion region. We make similar calculations for all the configurations of nucleon hole and pion particle states until the cross sections converge in the region of interest. The single particle states included in the calculations are $1f_{7/2} - 3p_{1/2}$ neutron-states (16 states) and $1f_{7/2} - 3s_{1/2}$ proton-hole states (10 states).

We show the calculated results in Fig. 5 leading to bound and unbound states. In this figure, we assume the energy resolution to be $1\text{MeV } FWHM$ which is an actual value of the (n,d) experiments. We will see, in the next section, more detail structure of the energy spectrum with better energy resolution which is realistic for the (d, ${}^3\text{He}$) reactions.

The cross sections in the bound pion region are similar to those published before.¹⁰ In the unbound region, we find still a significant amount of strength coming from bound pionic atom states coupled with neutron holes at higher excitation energy; $s - d - g$ shell with $h_{11/2}$ intruder, which begins at $E_x \sim 9\text{MeV}$ from the ground state of ${}^{207}\text{Pb}$. On the other hand, the difference between the negative pion spectrum and the neutral pion spectrum is remarkable as can be seen by comparing the curves with π^- and π^0 . The negative pion spectrum increases rapidly at the threshold, whereas the neutral pion spectrum only gradually increases from the threshold, which is 2.7MeV below the negative pion threshold. The small jump seen at 8MeV above the threshold in negative pion spectrum is caused by the beginning of the next neutron major shell with quasi-elastic pions. Adding all the contributions, we get the total cross sections as depicted by the thick solid curve. It is very interesting to note that the strength in the bound pion region is almost exclusively due to the bound pionic states. The peak appearing at $B_\pi \sim 5\text{MeV}$ mainly corresponds to the configurations $[l_\pi \otimes j_n^{-1}] = [2p \otimes p_{3/2}^{-1}]$ and $[2p \otimes p_{1/2}^{-1}]$ states.

Finally we overlay the calculated results on the experimental data, which is done in Fig. 6. To do so, we multiply a normalization factor $N = 1.7$ to the calculated results. This factor seems a reasonable value as the uncertainty of the effective number approach. We assume the flat background to be $0.28[\text{mb/sr/MeV}]$ which is not due to the pionic contribution. The agreement is remarkable. A small peak structure seen in experiment in the bound pion region might be identified to the similar structures

seen in the calculation.

4. Numerical Results on $(d, {}^3He)$ reactions

In this section, we compare our theoretical results with the data of the $(d, {}^3He)$ reactions taken at GSI ^{15,23}. We also show the spectrum with better energy resolution to predict what should be expected when experiments were performed with better energy resolution, and describe the underlying structures of the $(d, {}^3He)$ excitation functions. We show the energy dependence of the excitation function of the $(d, {}^3He)$ reaction with the ${}^{208}Pb$ target, too. For $(d, {}^3He)$ reactions, we only need to change reaction kinematics, elementary cross section, and distortion cross sections used in the eikonal approximation for the projectile and the ejectile from (n, d) cases described in section 2.

We show the calculated results on ${}^{208}Pb(d, {}^3He)$ reactions at $T_d = 600MeV$ in Fig. 7. In the upper part of Fig. 7, we show the forward cross sections with the resolution of 500 keV in order to compare with the experimental spectra shown in the middle part of Fig. 7. The agreement is almost perfect. We assume $20[\mu b/sr/MeV]$ flat background in the theoretical spectra. In order to see the underlying structures and also the spectra with a better experimental resolution, we show in the lower part of Fig. 7, the cross sections with 200 keV resolution. We can see now many peaks below the pion production threshold, which is denoted by the vertical dashed line. The peak seen experimentally consists of two states; $[l_\pi \otimes j_n^{-1}] = [p \otimes p_{1/2}^{-1}]$ and $[p \otimes p_{3/2}^{-1}]$. Since 4 neutrons are allowed in the $p_{3/2}$ state and 2 neutrons in the $p_{1/2}$ state, the ratio of the cross sections leading to $p_{3/2}^{-1}$ and $p_{1/2}^{-1}$ is 2. Those two states provide the peak and the shoulder structure at $Q = -136MeV$ (around 5MeV binding energy). The pionic s state seems to be only weakly excited due to the necessity of some momentum transfer. In addition, there is an appreciable amount of contribution from the neutron $f_{5/2}$ hole coupled to the pionic s state to this small peak. Many more peaks are seen closer to the pion production threshold. The dominant contributions are again coming from the pionic atom states coupled with the $p_{3/2}$ and $p_{1/2}$ neutron holes. It is interesting to comment on the bump structure seen in the calculated spectra around $Q = -143MeV$

in the continuum. This bump structure is caused by exciting $[1s_\pi \otimes s_{1/2}^{-1}]$ state, where a $s_{1/2}$ neutron in the $50 < N < 82$ major shell is picked up and a pion is placed in the $1s$ orbit. In the calculation, the neutron separation energy of the $s_{1/2}$ neutron hole state is calculated using the phenomenological potential ¹⁶ and width of the state is assumed to be zero since there is no experimental information.

We study now the energy dependence of the $(d, {}^3\text{He})$ cross sections. As could be guessed from the energy dependence of the elementary differential cross sections and that of momentum transfer, the $(d, {}^3\text{He})$ cross sections at different energies decrease. It is, however, interesting to see how the cross sections will change with the incident energy. For this purpose, we show the calculated results at $T_d = 500, 800$, and 1000MeV with the resolution of $\Delta E = 200\text{keV}$ and 500keV in Fig.8. As shown in the figures, the energy resolution of the cross section is essentially important to see the structure of deeply bound pionic states.

When we lower incident energy to $T_d = 500\text{MeV}$, the peak structure at $E \sim 5\text{MeV}$ is enhanced relative to other structure due to smaller momentum transfer. The peak structures are almost exclusively produced by the p neutron hole contribution. Note that the $1s$ pionic state is not appreciably excited at this energy. Those energy dependence are clearly explained by using the energy dependence of the calculated effective numbers.^{10,11} As the energy is increased to $T_d = 800\text{MeV}$, the cross sections are lowered. As indicated by the three kinds of curves in the spectrum with $\Delta E = 200\text{keV}$, now the contributions from the p neutron hole state become small, while the contributions from the $i_{13/2}$ and $f_{5/2}$ neutron hole states increase. Pionic states coupled with $f_{5/2}$ neutron hole state are excited appreciably. Further increased to $T_d = 1000\text{MeV}$, the peak structures are completely dominated by the $i_{13/2}$ neutron hole state coupled with various pionic atom states.

5. Conclusion

In this paper we have studied the (n, d) and $(d, {}^3\text{He})$ reactions on ${}^{208}\text{Pb}$ for the formation of deeply bound pionic states. We have calculated the formation cross sections for various cases and compared them with existing data. Our model is found to describe the reaction very well and has good predictive power as proven by the

fantastic agreement of newly obtained data to our prediction calculated before the experiments. We believe the model is a clue for the systematic studies of the structure and formation of deeply bound pionic states.

In order to develop the physics of deeply bound pionic atoms, we need to study the structure of pionic atoms more precisely by taking into account the configuration mixing effect of pion-particle neutron-hole state, the effect of nuclear deformation²⁴, and other effects. They may be important in deriving the pion mass in nuclear medium from the experiment²⁵. We also need to study the formation cross sections to other target nuclei to look for proper cases for observing the certain states of deeply bound pionic states²⁶. It is also interesting to study the formation of the deeply bound pionic states on unstable nuclei²⁷ using the same reaction model. We also mention that this direct reaction can be applied to the formation of other mesons such as η and ω inside nucleus to extract their properties at finite density²⁸.

6. acknowledgment

We acknowledge many discussions and collaborative works on the deeply bound pionic atoms with Prof. T. Yamazaki, Prof. R. S. Hayano and Dr. K. Itahashi. We also acknowledge stimulating discussions with Prof. K. Kume.

References

1. H. Toki and T. Yamazaki, *Phys. Lett.* **B213** (1988) 129.
2. H. Toki, S. Hirenzaki, T. Yamazaki, and R. S. Hayano, *Nucl. Phys.* **A501** (1989) 653.
3. M. Iwasaki *et al.*, *Phys. Rev.* **C43** (1991) 1099.
4. R. S. Hayano, *Proc. of Int. workshop on 'Pions in Nuclei', Penyscola, Spain* World Scientific (1991) 330.
5. J. Nieves and E. Oset, *Nucl. Phys.* **A518** (1990) 617.
6. J. Nieves and E. Oset, *Phys. Lett.* **B244** (1990) 368.
7. J. Nieves and E. Oset, *Phys. Rev.* **C43** (1991) 1937.
8. J. Nieves and E. Oset, *Z. Phys.* **A343** (1992) 477.
9. J. Nieves and E. Oset, *Phys. Lett.* **B282** (1992) 24.
10. H. Toki, S. Hirenzaki, and T. Yamazaki, *Nucl. Phys.* **A530** (1991) 679.
11. S. Hirenzaki, H. Toki and T. Yamazaki, *Phys. Rev.* **C44** (1991) 2472.
12. A. Trudel *et al.*, TRIUMF E628 and TRIUMF progress report (1991).
13. T. Yamazaki, *Nucl. Phys.* **A553** (1993) 221c.
14. N. Matsuoka *et al.*, *Phys. Lett.* **B359** (1995) 39.
15. T. Yamazaki *et al.*, *Z. Phys.* **A355** (1996) 219.
16. J. Speth, E. Werner, and W. Wild, *Phys. Rep.* **33** (1977) 127.
17. C. Richard-Serre, W. Hirt, D. F. Measday, E. G. Michaelis, M. J. M. Saltmarsh, and P. Skarek, *Nucl. Phys.* **B20** (1970) 413.
18. D. Aebischer, B. Favier, L. G. Greeniaus, R. Hess, A. Junod, C. Lechanoine, J. -C. Nikles, D. Rapin, and D. W. Werren, *Nucl. Phys.* **B106** (1976) 214.
19. J. Hoftiezer, Ch. Weddigen, B. Favier, S. Jaccard, P. Walden, P. Chatelain, F. Foroughi, C. Nussbaum, and J. Piaffaretti, *Phys. Lett.* **B100** (1981) 462.
20. H. W. Fearing, *Phys. Rev.* **C16** (1977) 313.
21. E. Aslanides, R. Bertini, C. Bing, F. Brochard, Ph. Gorodetzky, F. Hibou, T. S. Bauer, R. Beurtey, A. Boudard, G. Bruge, H. Catz, A. Chaumeaux, P. Couvert, H. H. Duham, D. Garreta, G. Igo, J. C. Lugol, M. Motoba, Y. Terrien, L. Bimbot, Y. LeBorne, and B. Tatischeff, *Phys. Rev. Lett.* **39** (1977) 1654.
22. K. Stricker, J. A. Carr, and H. McManus, *Phys. Rev.* **C22** (1980) 2043.

23. H. Toki, S. Hirenzaki, and K. Takahashi, *Z. Phys.* **A356** (1997) 359.
24. N. Nose-Togawa, S. Hirenzaki, and K. Kume, *Nucl. Phys.* **A** in press.
25. T. Yamazaki *et al.*, in preparation.
26. S. Hirenzaki and H. Toki, *Phys. Rev.* **C55** (1997) 2719.
27. H. Toki, S. Hirenzaki, and T. Yamazaki, *Phys. Lett.* **249B** (1990) 391.
28. S. Hirenzaki and H. Toki, in preparation

Table 1

Pion-nucleus optical potential parameters determined by Stricker *et al.*²²

$b_0[fm]$	-0.046
$b_1[fm]$	-0.134
$B_0[fm^4]$	$0.007 + 0.19i$
$c_0[fm^3]$	0.66
$c_1[fm^3]$	0.428
$C_0[fm^6]$	$0.287 + 0.93i$
λ	1.4
$k_F[fm^{-1}]$	1.4

Figure Caption

Fig. 1. Diagram for $(d, {}^3\text{He})$ reactions to form pionic bound states with a neutron-hole state.

Fig. 2. (a) The differential cross section $(d\sigma/d\Omega)^{lab}$ at 0 degree in the laboratory frame for $p(p, d)\pi^+$ as a function of the incident energy T_p , derived from the experimental values of $(d\sigma/d\Omega)^{c.m.}$ for $p(p, \pi^+)d$.¹⁰ The data are taken from references^{17,18,19}. The solid line is the phenomenological fit to the data.¹⁰ (b) The differential cross section $(d\sigma/d\Omega)^{lab}$ at 0 degree for $p(d, t)\pi^+$ as a function of the incident energy $T_d/A[\text{MeV}/\text{nucleon}]$, derived from the experimental values for $d(p, \pi^+)t$.^{20,21} The solid curve is obtained by multiplying 1.7 to the theoretical result of Fearing²⁰ to match the experimental cross sections.

Fig. 3. The negative and neutral pion wave functions relative to ${}^{208}\text{Pb}$ at $T_\pi = 5\text{MeV}$ for $l_\pi = 0$. (a) The wave functions without the optical potential. (b) The wave functions calculated with optical potential, which reproduce the elastic pion scattering data.

Fig. 4. Quasi-elastic pion production cross sections in (n, d) reactions for a negative pion with $p_{3/2}$ neutron hole and those for a neutral pion with a $d_{5/2}$ proton hole. The zero is the threshold energy for each case.

Fig. 5. ${}^{208}\text{Pb}$ reaction cross sections at zero degree leading to deeply bound pionic atoms and quasi-elastic pionic states calculated within the effective number approach. The horizontal axis, π Binding Energy, is defined to be 0MeV at the π^- production threshold with the ground state of ${}^{207}\text{Pb}$ and it corresponds to $Q = -143.4[\text{MeV}]$ for (n, d) reactions. We take 1MeV FWHM as an instrumental resolution.

Fig. 6. ${}^{208}\text{Pb}(n, d)$ reaction cross sections at zero degree at $T_n = 400\text{MeV}$. The solid curve is the calculated result with a normalization factor of 1.7. The flat background is assumed to be $280[\mu\text{b}/\text{sr}/\text{MeV}]$. We take 1MeV FWHM as an instrumental reso-

lution. The horizontal axis is defined as in Fig. 5.

Fig. 7. Forward cross sections of the $^{208}Pb(d,^3He)$ reaction at $T_d = 600MeV$; (a) Theoretical results with the experimental resolution of $500keV$, (b) Observed spectrum by Yamazaki *et al.*¹⁵, and (c) Theoretical results with $200keV$ experimental resolution. In (a) and (c) the flat background is assumed to be $20[\mu b/sr/MeV]$. The vertical dashed line denotes the π^- emission threshold energy.

Fig. 8. Calculated cross sections of the $^{208}Pb(d,^3He)$ reaction at (a) $T_d = 500MeV$, (b) $T_d = 800MeV$, and (c) $T_d = 1000MeV$ with $200keV$ (left) and $500keV$ (right) experimental energy resolution. Solid curves show the full spectra including all contributions. Dotted curves show the contributions from the neutron $2p$ states ($p_{3/2}$ and $p_{1/2}$) and dashed curve show those from the neutron $i_{13/2}$ state. Added is also the contribution from the neutron $1f$ states ($f_{5/2}$ and $f_{7/2}$) by dash-dotted curve in the middle figure.

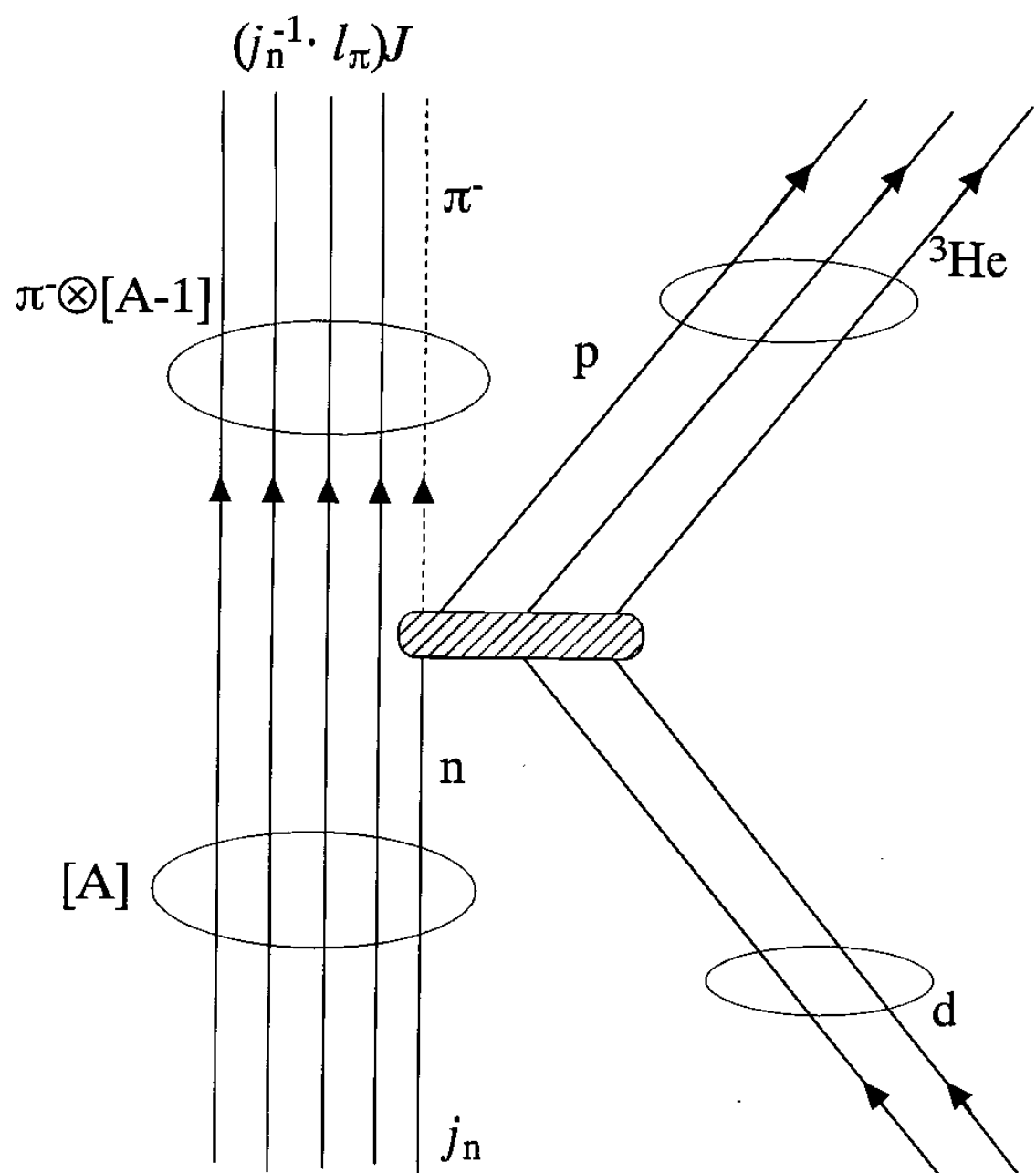


Fig. 1

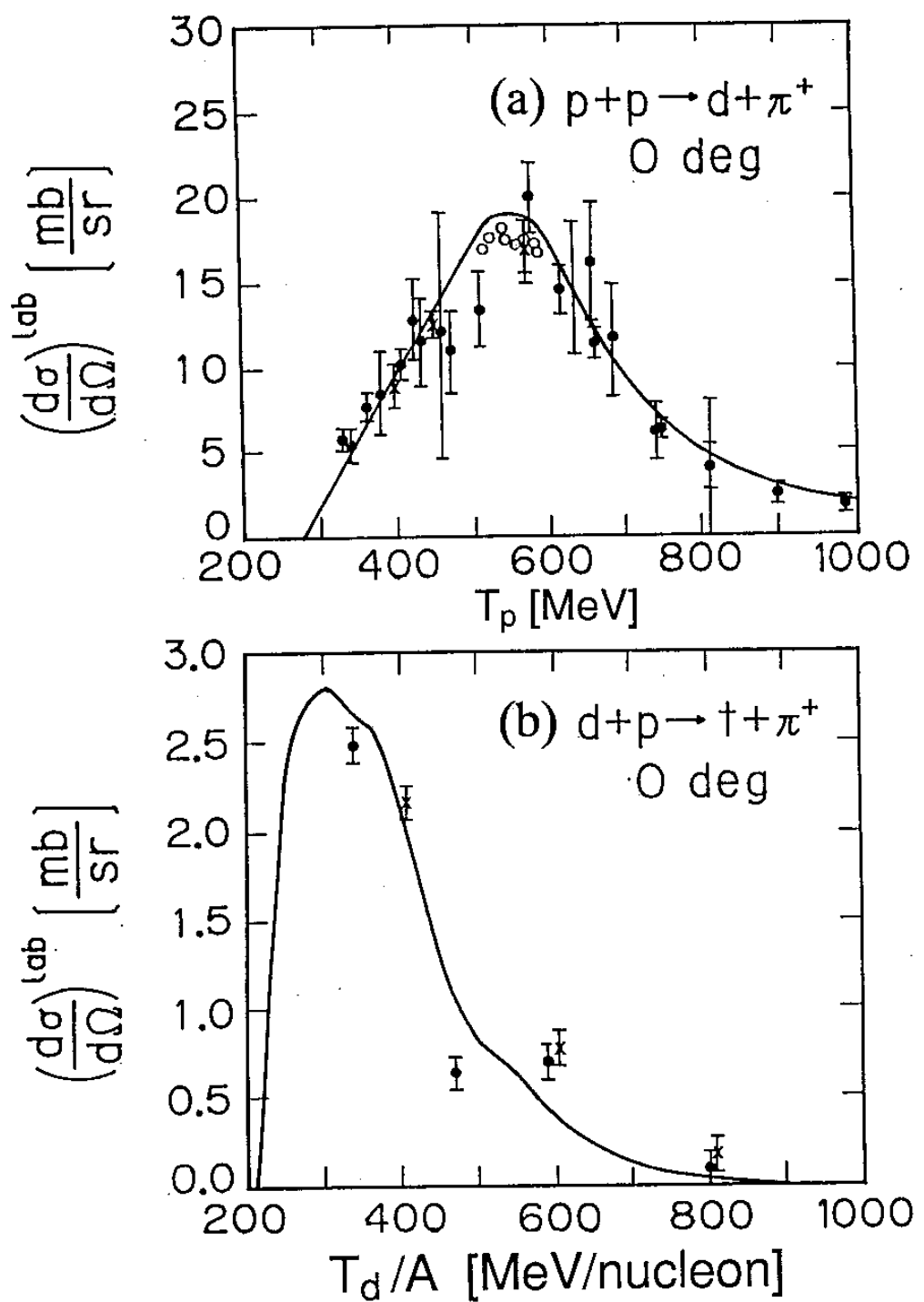


Fig. 2

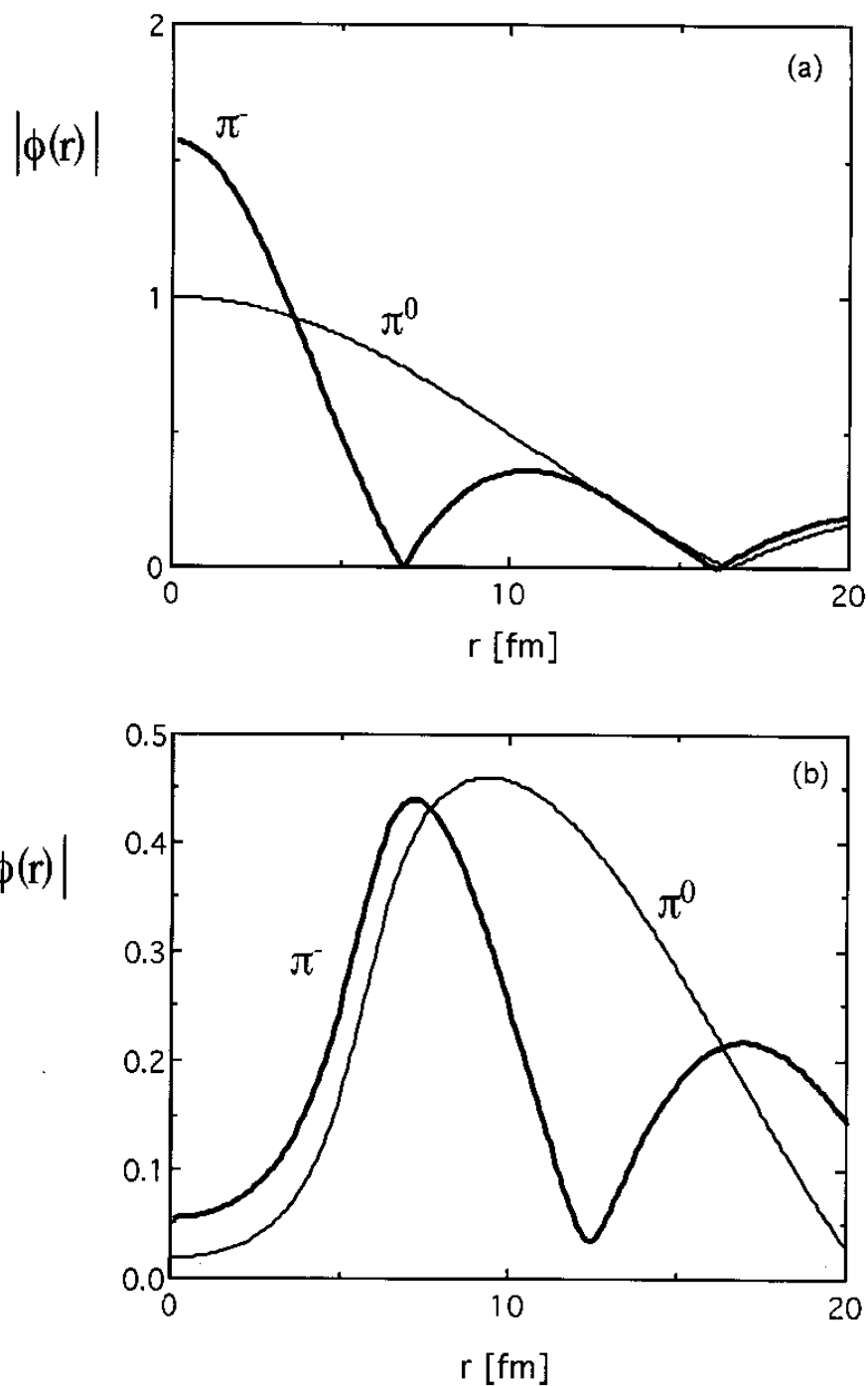


Fig. 3

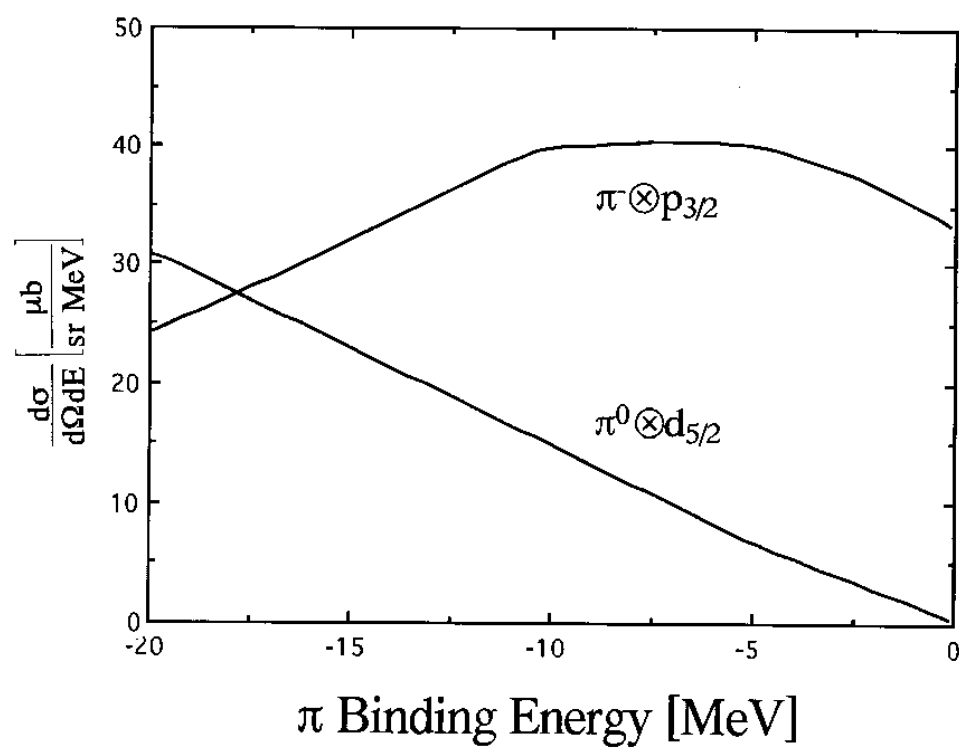


Fig. 4

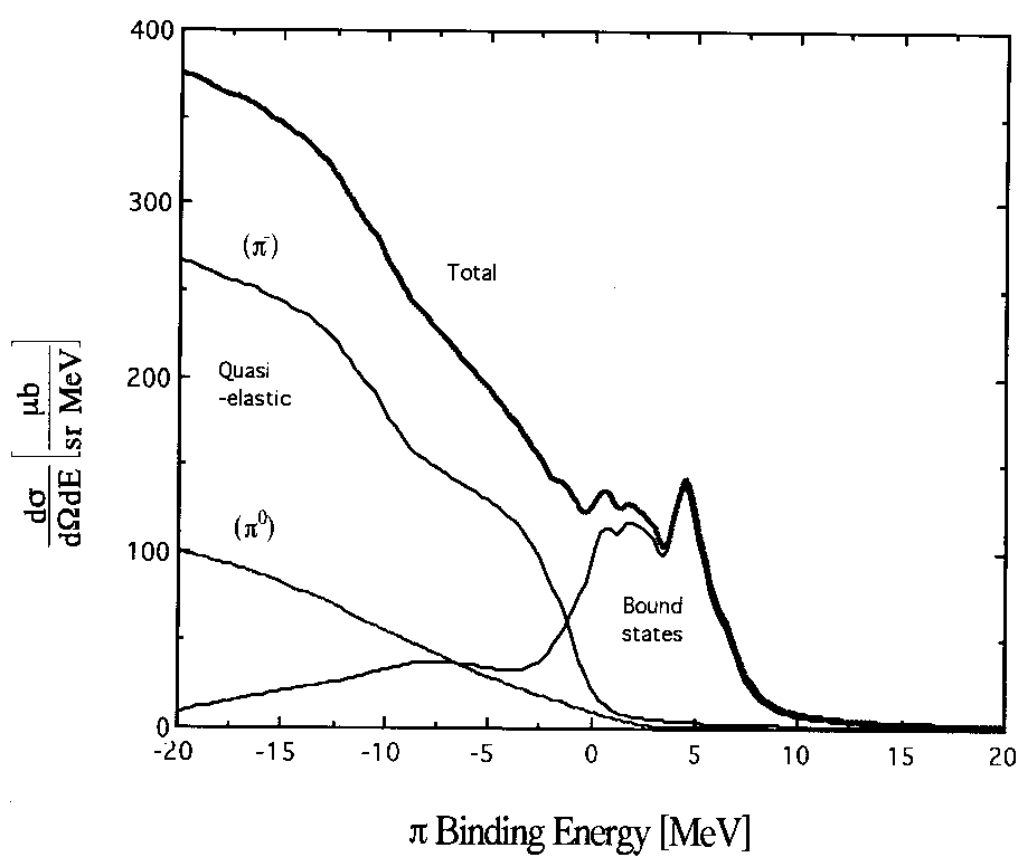


Fig. 5

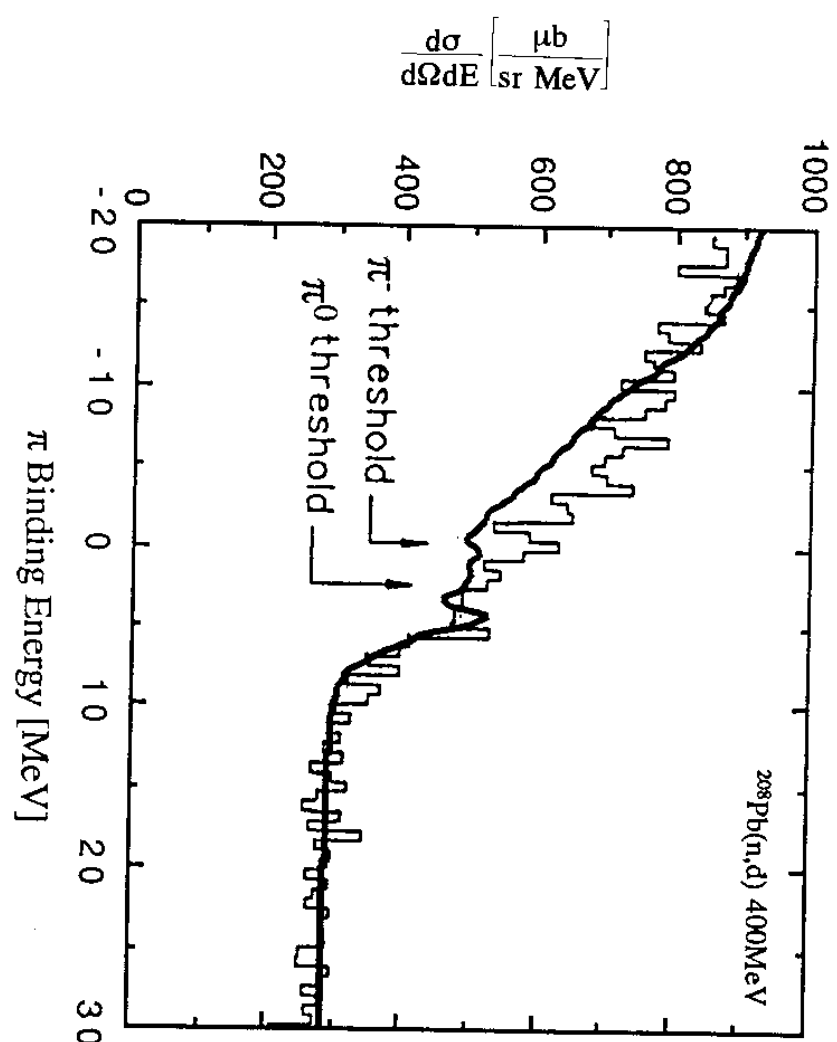


Fig. 6

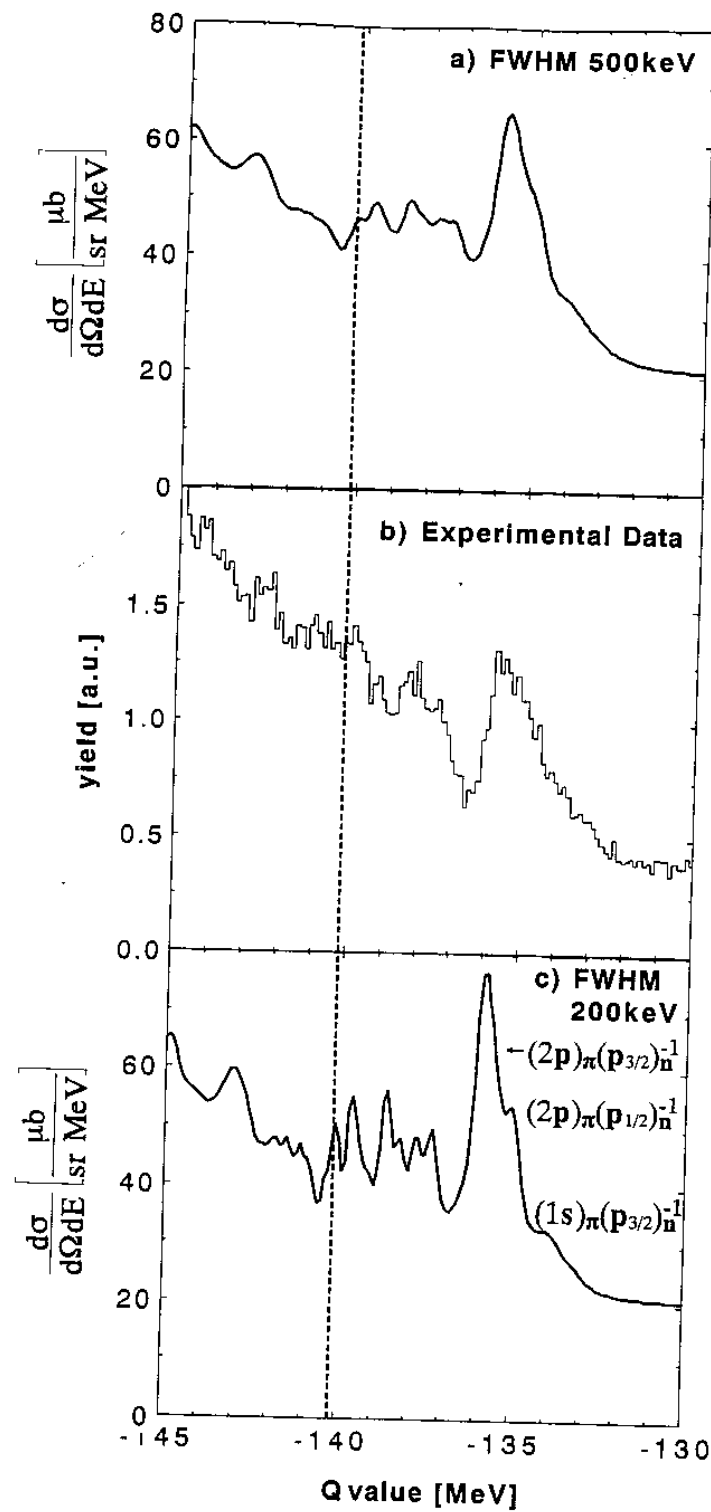


Fig. 7

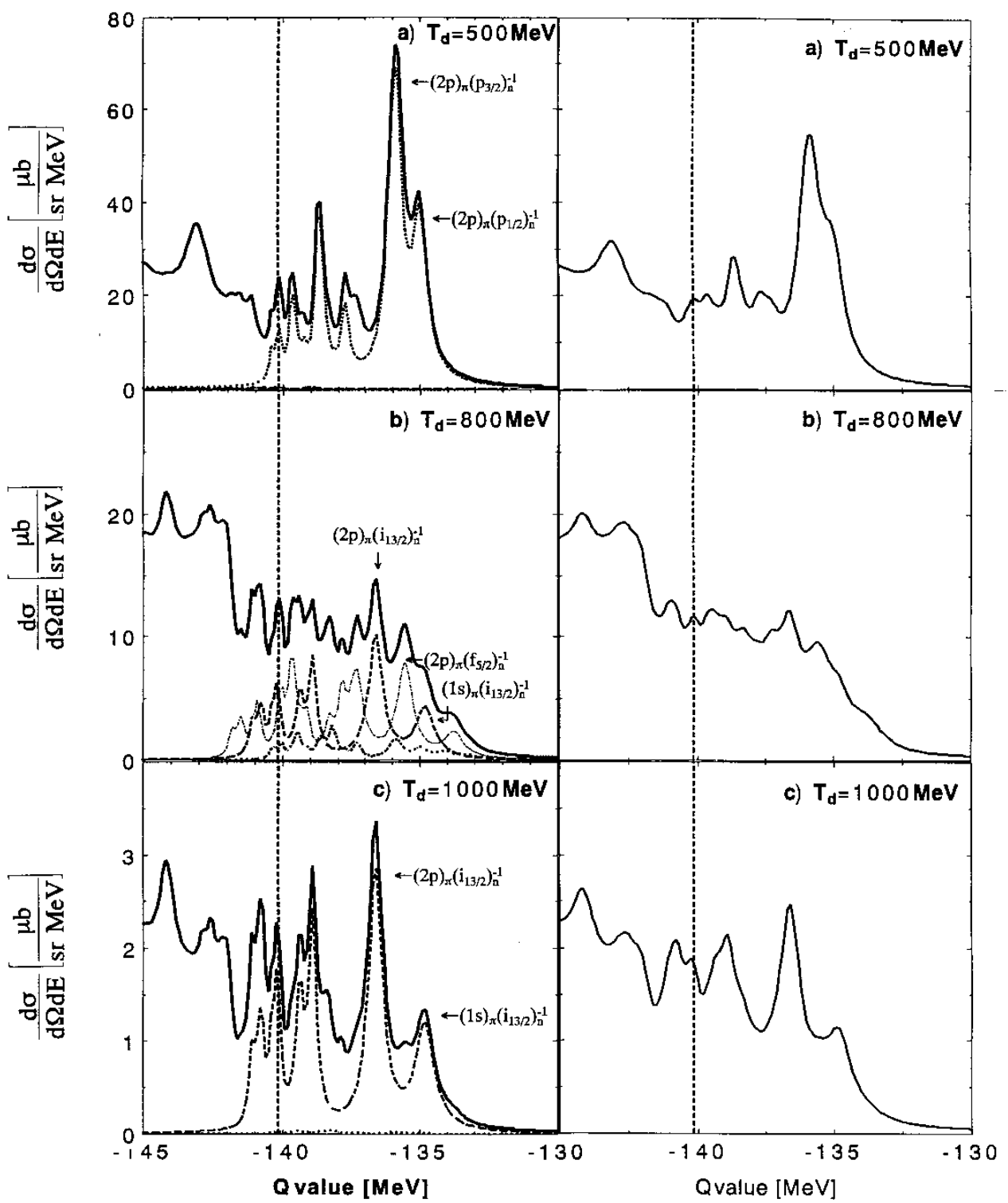


Fig. 8